Miniaturised Soft Manipulators with Reinforced Actuation Chambers on the Sub-centimetre Scale

Jialei Shi[1], Sara-Adela Abad[1,4], Arianna Menciassi[2], Kaspar Althoefer[3], and Helge A. Wurdemann[1]

***Abstract*— Fibre-reinforced soft robots are often considered in the design of fluid elastomer actuators, to counter ballooning and potential bursting when exposed to high levels of pressure. They also enhance deformation and navigation through confined spaces. These attributes are critical in applications such as minimally invasive surgical (MIS) procedures that use sub-12 mm diameter trocar ports. While soft robots with fully reinforced actuation chambers have not yet attained this level of miniaturisation, this paper outlines the fabrication and characterisation of miniaturised soft manipulators with reinforced actuation chambers on the sub-centimetre scale (i.e., less than 10 mm). Two robots are presented with diameters of 9.5 mm and 7.8 mm. They have four pneumatic actuation chambers per robotic segment, with a free central working lumen. Additionally, two robotic segments are serially connected to enhance dexterity and flexibility. This research advances the miniaturisation of soft manipulators with reinforced chambers and an inner free lumen, enhancing their use in applications within confined and unstructured environments.**

I. Introduction

The fundamental working principle of fluidic-driven soft robots is to pneumatically or hydraulically pressurise cavities within soft material structures. The exhibited an-isotropic strains result in shape changes such as bending, contracting, elongating and twisting [1]–[3]. Fibre-reinforced fluid soft robots use (in)extensible fibres. These fibres are either embedded within the whole soft elastomeric structure or integrated into specific regions [4], to constrain certain deformation strains when soft robots are actuated. By way of example, fibre reinforcement can prevent soft robots from ballooning when subjected to high levels of actuation pressure [5].

The concept of fibre-reinforced actuators effectively dates back to the 1950s when McKibben Artificial Muscles, also know as pneumatic artificial muscles, were primarily developed for orthotic applications [6]. The outermost layer of McKibben Muscles consists of double-helix-braided sheaths. When the inner bladder is pressurised, the artificial muscle contracts (braided angle $\leq 54°44'$) or elongates (braided angle $\geq 54°44'$) [7]. Another landmark in the advancement of fibre-reinforced soft actuators can be attributed to the flexible micro-actuators (FMAs) developed in the 1990s [8]. FMAs comprise fibre-reinforced rubber and have three chambers actuated by pressurised fluids. The diameters of these FEAs range from 1 mm to 12 mm [9], making them suitable for a broad spectrum of applications, including walking robots and soft grippers. FMAs brought about the design paradigm of reinforcing entire robot bodies, thereby inspiring inventions such as soft swimming fishes [10], marine soft gripper [11], rotary actuators [12], soft medical instruments [13], and bending actuators [14]. Notably, the research in [5] studied the relationship between the fibre angle and the resulting deformation of the pressurised fibre-reinforced actuators. It is demonstrated that the responses of soft actuators can be mechanically programmed by adjusting the angle of the fibres. Nevertheless, reinforcing the entire actuator could lead to interference of the actuated chambers and sensing difficulties, particular for soft actuators with multiple actuation chambers [15]. For instance, the cross-sectional area and the centre position of chambers could vary as a result of pressurisation. In such situations, the bending of soft actuators depends on both the pressure level in chambers and number of pressurised chambers [16].

To address these limitations, the concept of reinforcing each individual chamber is proposed. The OctArm, for example, was designed in [17] to achieve high-payload manipulation. The robot has three robotic segments, with each segment comprising three reinforced chambers or chamber

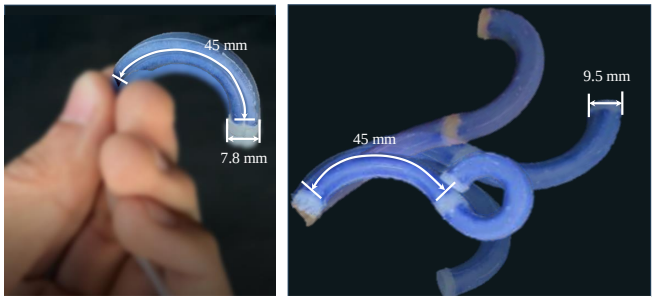

(a) (b)

Fig. 1. Miniaturised soft manipulators on the sub-centimetre scale. The soft robots have fully reinforced actuation chambers while retaining a central free lumen. (a) A one-segment robot with a diameter of 7.8 mm. (b) A two-segment robot with a diameter of 9.5 mm.

This work is supported by the Springboard Award of the Academy of Medical Sciences (grant number: SBF003-1109), the Engineering and Physical Sciences Research Council (grant numbers: EP/R037795/1, EP/S014039/1 and EP/V01062X/1), the Royal Academy of Engineering (grant number: IAPP18-19\264), the UCL Dean's Prize, UCL Mechanical Engineering, and the China Scholarship Council.

[1]J. Shi, S. A. Abad, and H. A. Wurdemann are with the Department of Mechanical Engineering, University College London, WC1E 6BT, UK. (e-mail: jialei.shi.19@ucl.ac.uk, h.wurdemann@ucl.ac.uk).

[2] A. Menciassi is with the BioRobotics Institute and with the Department of Excellence in Robotics & AI, Scuola Superiore Sant'Anna, 56127 Pisa, Italy. (e-mail: arianna.menciassi@santannapisa.it).

[3] K. Althoefer are with the Centre of Advanced Robotics @ Queen Mary (ARQ), Faculty of Science and Engineering, Queen Mary University of London, London E1 4NS, UK. (e-mail: k.althoefer@qmul.ac.uk).

[4] S. A. Abad is also with the Institute for Applied Sustainability Research, Quito, Ecuador. (email: s.abad-guaman@ucl.ac.uk).

CROSS-SECTIONAL DIMENSION OF TWO SOFT ROBOTS

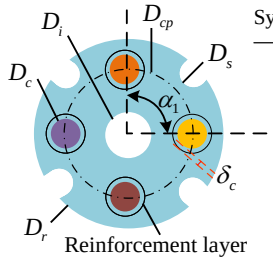

Symbol	Description	Dimensions of 9.5 mm robot	Dimensions of 7.8 mm robot	Units
D_r	Diameter of the soft robot	9.5	7.8	[mm]
D_i	Diameter of the central lumen	2.5	2	[mm]
D_c	Diameter of the actuation chambers	1.5	1	[mm]
D_{cp}	Diameter of the chamber position	6	5	[mm]
D_s	Diameter of the slots	1.5	1.5	[mm]
α_1	Angle between two adjacent chambers	90.0	90.0	[deg]
δ_c	Wall thickness of the chambers	0.5	0.4	[mm]

Fig. 2. Cross-sectional geometries of two miniaturised soft robots. Each robotic segment has four independent actuation chambers while retaining a free central lumen.

pairs. Multi-segment fluidic soft robots controlled by human-powered masters were proposed in [18] and intended for underwater tasks. Similarly, each robotic segment had three reinforced chambers. The inherent compliance and consequent flexibility of soft robots also offers valuable benefits for medical interventions [19], [20]. Another prominent example is the STIFF-FLOP manipulator devised for MIS [21]–[23]. Broadly speaking, this manipulator is a cylindrical robotic device made of silicone, with fully reinforced chambers and a central lumen [15]. The diameter of the manipulator, when miniaturised, ranges from 14 mm to 15 mm [24], [25]. A key finding was that the shape of the reinforced chamber significantly influences the kinematics, stiffness and force generation of the soft robot [26]. Inspired by the STIFF-FLOP design, a two-segment soft instrument was designed in [27], envisioned for cancer imaging and controlled using the Simulation Open Framework Architecture (SOFA), a software specifically developed for implementing FEM-based simulation and control. This soft instrument has a diameter of 11.5 mm with three reinforced chamber pairs [28].

Medical applications, such as endoscopic interventions, usually use trocar with diameters smaller than 12 mm [29]. Consequently, soft medical instruments need to be on the sub-centimetre scale (i.e, smaller than 10 mm) [30]. The challenge therefore lies in miniaturising the dimensions of soft robots while retaining their individually reinforced chambers and working lumen [31]. As previously noted, the diameters of existing STIFF-FLOP manipulators are between 14 mm and 15 mm, potentially restricting their suitability for MIS applications. As such, the contribution of this paper lies in the miniaturisation of soft robots with reinforced chambers, with thorough characterisation of their static and dynamic performances. For the first time, we create these robots on the sub-centimetre scale (i.e., less than 10 mm). The achieved miniaturisation relies on an improved fabrication process with fewer moulds (see Fig. 3), where metal rods and a silicone injection technique are introduced. This paper presents and characterises miniaturised two-segment soft robots, with diameters of 9.5 mm and 7.8 mm. Each segment has four independent pneumatic actuation chambers and a central working lumen, as illustrated in Fig. 1.

The remainder of this paper is organised as follows: Section II details the robot fabrication process. Section III presents the experimental characterisation and comparison of the two robots, with a focus on kinematics, force capability, dynamics and robustness to withstand extreme pressure. The discussions and conclusions of this paper are reported in Section IV and Section V, respectively.

II. DESIGN AND FABRICATION OF MINIATURISED SOFT MANIPULATORS

A. Dimension Requirements of Soft Robots

A trocar is a medical instrument with a sharply pointed end and a hollow cylinder (cannula), for the purpose of introducing ports into the abdomen. For endoscopic interventions, trocars are available in different sizes, generally ranging from 3 mm to 12 mm. Trocar ports can be dilated to larger than 12 mm, such as when larger tumours need to be extracted [32]. In standard procedures, the ideal trocar diameter is less than 10 mm [29]. In view of this, our work aims to create two soft robots (see Fig. 1) on the sub-centimetre scale, aligning with the dimensions of trocar ports in standard clinical procedures. Cross-sectional dimensions of the two robots are in Fig. 2.

B. Robot Fabrication

The fabrication process for the two miniaturised robots reported in this work is summarised in Fig. 3. As shown in Fig. 3(a), the body moulds, sealing moulds and end moulds are 3D-printed. Instead of utilising 3D-printed rods as chamber moulds, which may result in shape deflection and rigidity issues, metal rods are employed. These metal rods comprises bigger and smaller sizes to create the outer and inner layer of reinforced chambers. The diameter of the bigger rods for the 9.5 mm and 7.8 mm robots is 2.5 mm and 2 mm, respectively. In addition, the corresponding diameter of the smaller rods for two robots is 1.5 mm and 1.0 mm, respectively. The reinforcement layer is then created by wrapping thread around the bigger metal rods, as depicted in Fig. 3(b). The body moulds, bigger moulds with reinforcement, and end moulds for bigger rods are then assembled. Fig. 3(c) illustrates the two silicone curing steps. Initially, silicone [Ecoflex 50, Smooth-On] is injected into the assembled moulds. The bigger metal rods are then taken out once the silicone has cured. The inner chamber layer is created by injecting silicone and then inserting a smaller

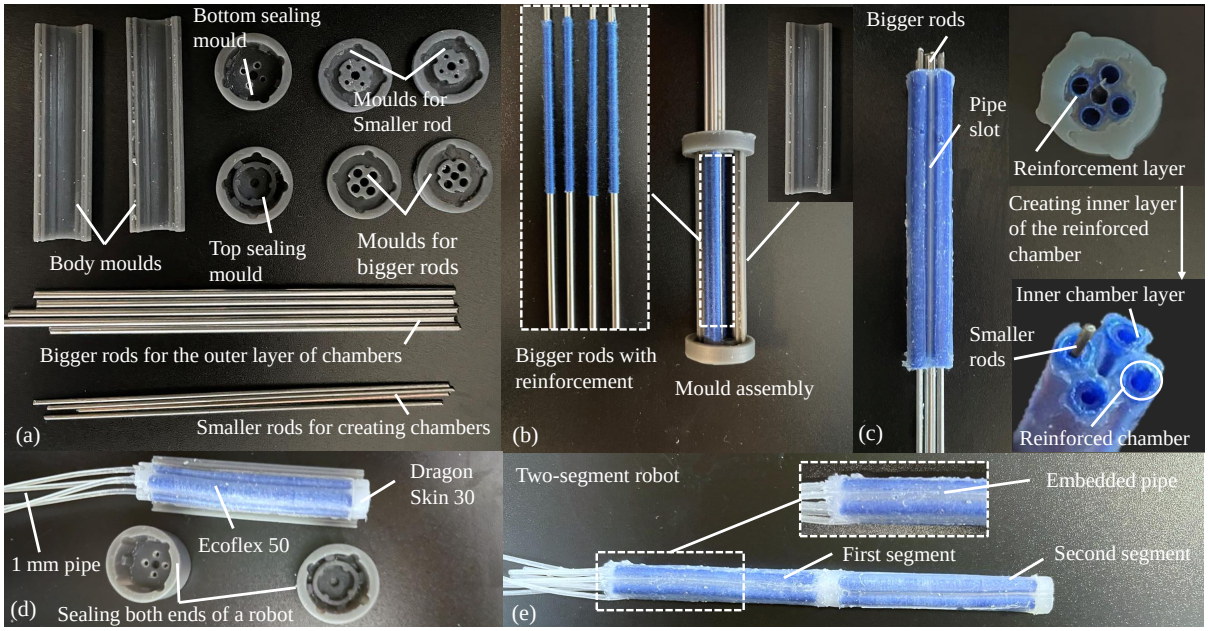

Fig. 3. Fabrication process of the miniaturised soft robots, illustrated using the 7.8 mm robot. (a) Printed moulds and metal rods. (b) Moulds are assembled after the reinforcement threads are wrapped around the metal rods. (c) Fabricated robot with reinforced chambers. (d) Sealing both ends of the robot using Dragon Skin 30. (e) A complete two-segment robot, where the actuation pipes from the second robotic segment are embedded into the slots of the first robotic segment.

metal rod into each chamber. In Fig. 3(d) we see that both ends of the fabricated robots are sealed using Dragon Skin 30, while the actuation pipes are glued to one end of the robot. Lastly, we see how two robotic segments can be connected serially. To preserve a free central lumen, actuation pipes from the second segment are embedded into the slots of the first segment, as demonstrated in Fig. 3(e).

III. Experimental Characterisation and Comparison of Two Soft Robots

A. Experimental Hardware

The chamber pressure is regulated by proportional pressure regulators (Camozzi K8P). A compressor (HYUNDAI HY5508) supplies pressurised air to the pressure regulators which are controlled via analogue signals by an Arduino DUE. An electromagnetic tracking system (NDI Aurora) monitors the tip position/orientation of the soft robots. The sampling frequency of the Aurora tracking system is 40 Hz. MATLAB communicating with the Arduino DUE is used to send pressure and record data. Details of the experimental hardware are reported in [33].

B. Experimental Protocols

Experiment 1 - Bending and Elongation of Robots: A 6-DoF magnetic NDI tracker allows measurement of both elongation displacements and bending angles. The elongation ratio is a dimensionless quantity and computed as the displacement along the z-axis divided by the original robot length. In the elongation test, the four chambers were simultaneously actuated. In the bending test, one, two, or three chambers were actuated. The maximum actuation pressure was set at 1.5 bar, 1.2 bar and 1.0 bar when the first, second, and both robotic segments were actuated, respectively. Each test was repeated over three trials.

Experiment 2 - Payload Capability: The payload capability was evaluated based on the lifting height Δz achieved by actuated soft robots when presented with tip loads (see Fig. 5). Payloads of 0g, 1g, 2g, 3g, 4g, and 5g, were applied at the tip of two robots while they generated in-plane and out-of-plane bending motions. Please note that the terms 'in-plane' and 'out-of-plane' refer to that the backbone of a soft robot bends within a single plane as well as through different planes [34]. Throughout all tests, the actuation pressure was set at 1.2 bar. In the in-plane bending tests, the first, second, and both segments were tested, while in the out-of-plane bending tests, both segments were actuated simultaneously.

Experiment 3 - Robot Dynamics: The dynamic response of the robot in terms of bending and elongation was characterised when the first, second and both segments were actuated. Each test spanned a duration of 15 seconds, with a step pressure of 1.0 bar introduced at the fifth second. In the bending tests, one, two and three chambers were actuated, while in the elongation tests, all four chambers were actuated. The elongation and bending angle of the robots were measured by the tracker.

Experiment 4 - Burst Pressure Evaluation: To evaluate the robustness of the fabricated robot under extreme conditions, a burst pressure test was conducted on the smaller (7.8 mm diameter) robot. The actuation pressure was applied linearly from 0 bar to a regulated maximum of 3.0 bar in 10 seconds.

C. Experimental Results

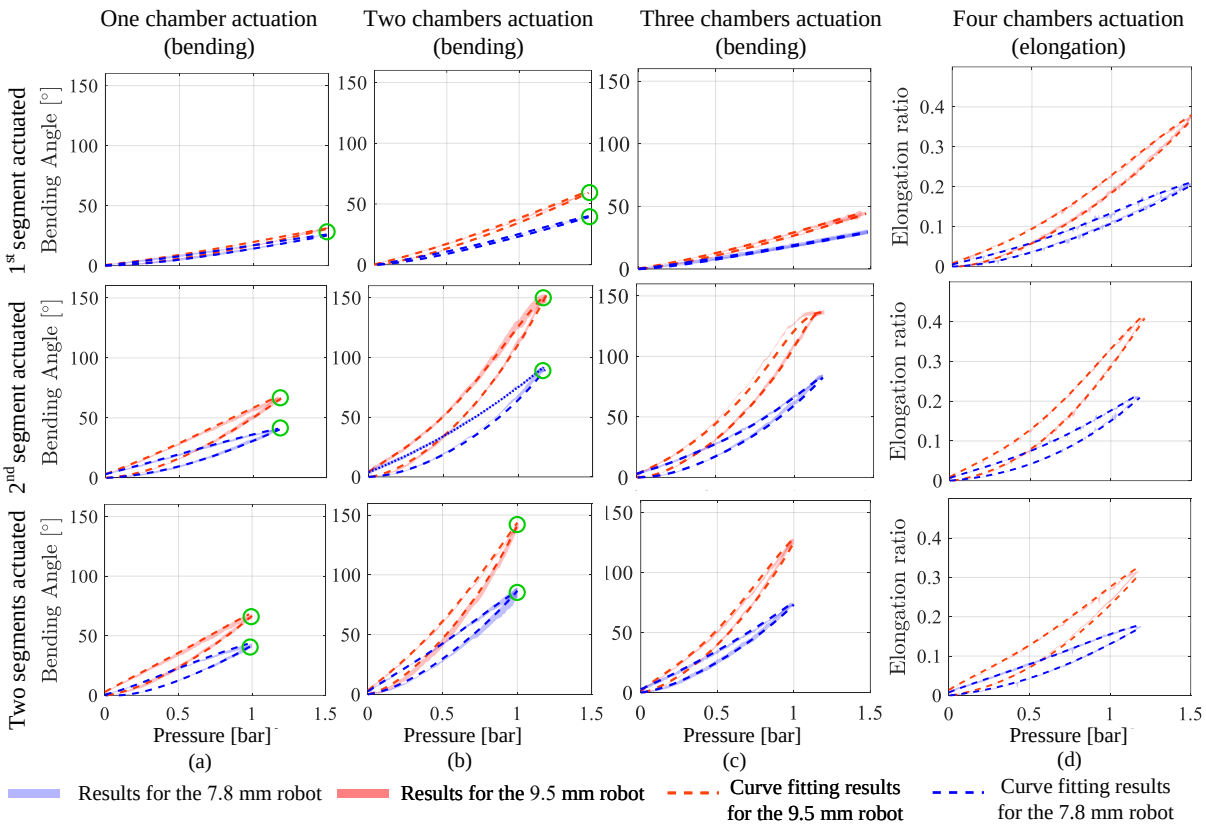

Fig. 4. Results for Experiment 1: Bending and elongation of two robots when (a) one, (b) two, (c) three and (d) four chamber(s) are actuated. The characterisation results when the first, the second, and both robotic segments are actuated are reported from the top row to the bottom row, respectively.

Results for Bending and Elongation of Robots: Fig. 4 presents the characterisation results for the elongation and bending tests. Fig. 4(a) reports the tip bending angle versus the actuation pressure when one chamber is actuated. The results of both robots demonstrate that, for the same actuation pressure, the bending angle produced by the second segment is larger than that from the first segment. For instance, the average bending angle of the 7.8 mm robot is 20.6°, but 39.7° when actuating one chamber of the first and second segment under pressure of 1.2 bar. Given the same actuation conditions, the first and second segment of the 9.5 mm robot produces bending angles of 23.3° and 67.3° respectively. In contrast, when both segments are actuated simultaneously, these robots can achieve bending motion under lower pressures. Indeed, the 7.8 mm and 9.5 mm robots can generate equivalent bending angles of 43.2° and 67.7° when the pressure is 1.0 bar. Under the same actuation pressure, Fig. 4(b) demonstrates that bending angles resulting from two chamber actuation are about twice as large, as highlighted by the green circles in Figs. 4(a)-(b). For instance, the average bending angles for the 7.8 mm and 9.5 mm robots are 88.2° and 143.1° respectively, when two segments are actuated. Moreover, Fig. 4(c) illustrates the bending angle under different pressures when three chambers are actuated. Overall, we observe that bending angles produced by the actuation of three chambers do not exhibit an increase, but rather a decrease of 10°∼15° when compared to results from Fig. 4(b) with the pressure at 1.5 bar. As the maximum pressure varies from 1.2 bar to 1.5 bar, Fig. 4(d) illustrates that the elongation ratios for the 7.8 mm robot and 9.5 mm robot are within the ranges of 0.15∼0.22 and 0.30∼0.40, respectively. To conclude these results, the 9.5 mm robot

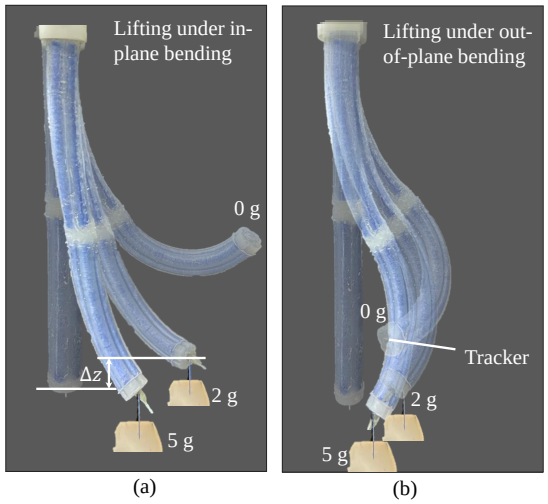

Fig. 5. Illustration of the payload characterisation in Experiment 2. Lifting various tip loads when the robot generates (a) in-plane and ((b) out-of-plane bending motions.

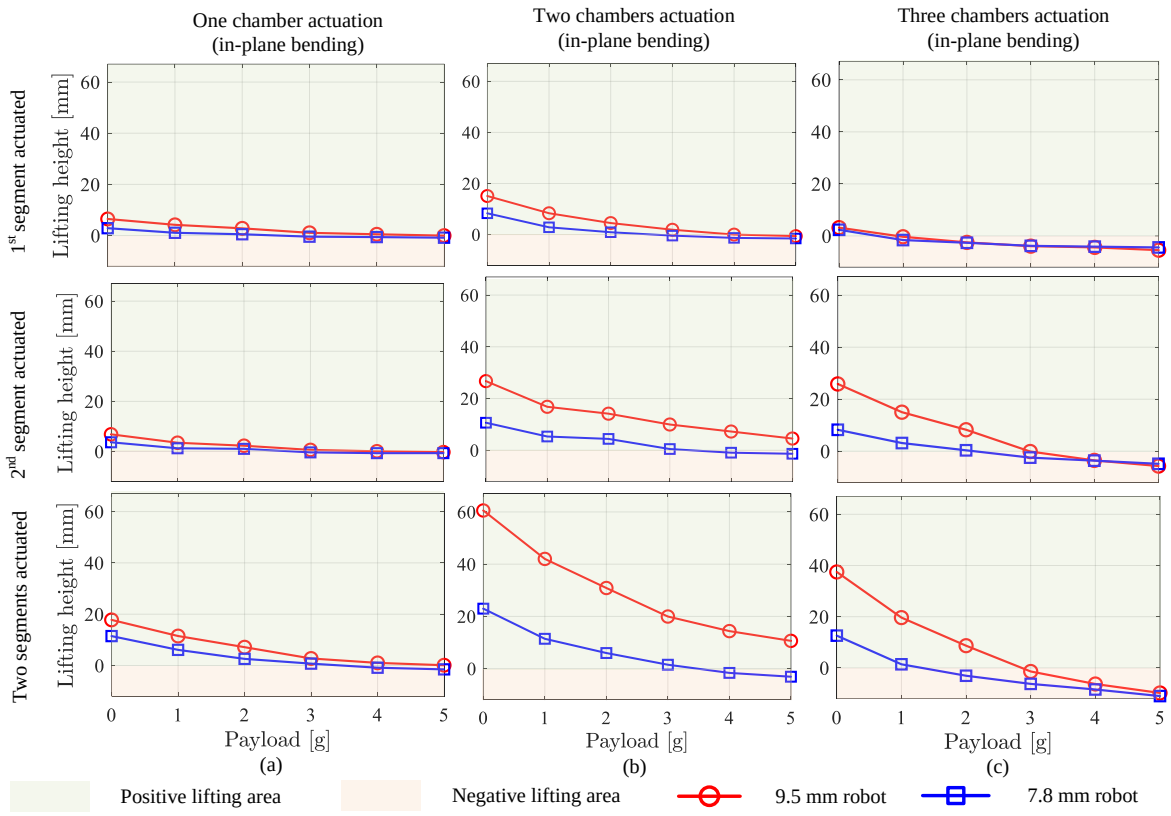

Fig. 6. Result for Experiment 2: Lifting height when two robots generate in-plane bending motions (see Fig. 5(a)), with 0 g, 1 g, 2 g, 3 g, 4 g, and 5 g loads applied at the robot tip. The results when (a) one chamber, (b) two chambers and (c) three chambers are actuated.

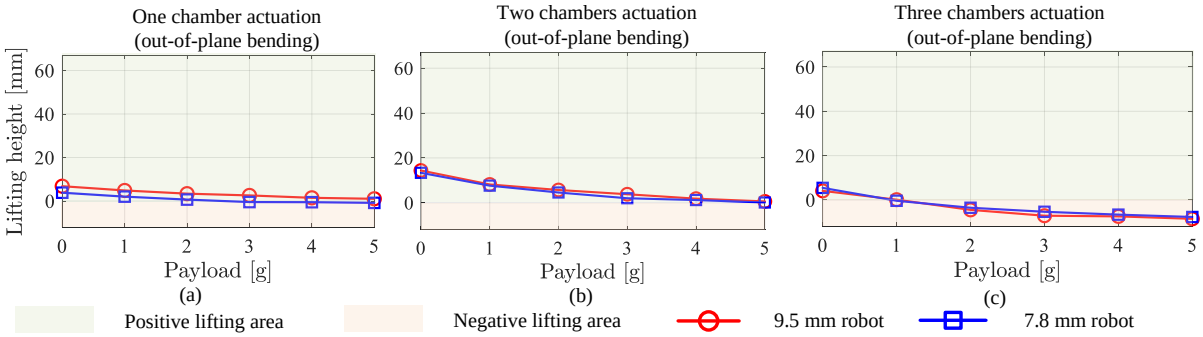

Fig. 7. Result for Experiment 2: Lifting height when two robots generate out-of-plane bending motions (see Fig. 5(b)) by actuating two segments simultaneously. 0 g $\sim$ 5 g loads are applied at the robot tip. The results when (a) one chamber, (b) two chambers and (c) three chambers are actuated.

needs less pressure to generate a similar bending angle or elongation distance than the 7.8 mm robot in all tests.

Results for Payload Capability: Figs. 5(a) and (b) illustrate the lifting height Δz in the in-plane and out-of-plane bending tests, as exemplified by the 7.8 mm robot. It is important to highlight that Δz is only positive when the position of actuated robot tip is higher than the tip position when not actuated. If this is not the case, the Δz value is negative. In Figs. 6 and 7, positive and negative lifting heights are denoted by green and pink backdrop colours, respectively.

Fig. 6 sets out the results when the two robots generate in-plane bending motions. Fig. 6(a) summarises the results when one chamber is actuated. When applying various loads, the results demonstrate that the 9.5 mm robot exhibits higher lifting heights, i.e., a superior payload capacity, than the 7.8 mm robot. However, the lifting height of the two robots converge to zero when payloads are larger than 3 g. Fig. 6(b) reveals that the overall payload capability of the robots increases when two chambers are actuated, unlike the results from one chamber actuation in Fig. 6(a). For example, when the payload is 2 g, the lifting heights for the 9.5 mm and 7.8mm robots are 30.9 mm and 6.0 mm respectively. By contrast, the corresponding lifting height is 7.1 mm and 2.6 mm from Fig. 6(a), under the same payload conditions. Moreover, a lower force capability is then observed from Fig. 6(c) when moving from two to three actuated chambers.

TABLE I

RESULTS FOR EXPERIMENT 3: IDENTIFIED DYNAMIC PARAMETERS FOR TWO ROBOTS.

System type	Actuated segment	Diameter	One chamber actuated				Two chambers actuated				Three chambers actuated				Four chambers actuated			
			k	a	b	c	k	a	b	c	k	a	b	c	k	a	b	c
Third-order $\frac{k}{s^3+as^2+bs+c}$	Both segments	9.5 mm	94750	9.9	322.3	1359	139200	9.7	251.1	956.2	91600	11.4	214.3	692.1	9586	8.6	191.7	606.5
			96.13%				97.21%				95.98%				95.01%			
		7.8 mm	86350	11.5	343.1	1738	116400	10.4	299.7	1265	71160	11.4	226.8	874.2	7248	10.78	240.9	847
			96.27%				96.57%				96.16%				95.32%			
	1st segment	9.5 mm	47090	10.0	328.9	2258	67950	9.33	272.9	1988	44000	9.0	234.6	1788	7286	12.58	333.8	1133
			92.51%				91.89%				91.61%				95.52%			
		7.8 mm	42890	13.1	368.7	3306	62650	11.3	311.5	2483	40200	9.7	282.5	2252	4588	11.42	289.3	1142
			90.21%				92.84%				89.31%				95.45%			
Second-order $\frac{k}{s^2+as+b}$	2nd segment	9.5 mm	3916	20.7	75.4	–	7288	19.2	61.9	–	5615	14.9	48.8	–	794.6	23.64	82.7	–
			94.85%				95.34%				95.73%				95.17%			
		7.8 mm	2156	17.5	66.4	–	4192	16.0	60.4	–	4519	16.2	66.1	–	411.8	23.75	94.01	–
			94.85%				96.21%				95.53%				95.34%			

* Results reported in blue cells denote values of "Fit to estimation data" from the Maltab System Identification Toolbox.

In particular, Δz exhibits larger negative values (e.g., up to -10 mm) when the payload increases, especially in the case of the 7.8 mm robot.

Fig. 7 sets out the results when the two robots generate out-of-plane bending motions, with two segments both actuated. Similar to the results in Fig. 6, Fig. 7(b) illustrates that both robots exhibit the best force capability when two chambers are actuated. The force capability of the robots are closer to each other in Fig. 7 for out-of-plane bending motions, as compared to the results from Fig. 6 for in-plane bending motions. Furthermore, all the lifting heights of both robots in Fig. 7 are below 20 mm, which is lower than the lifting heights achieved in Fig. 6. Additionally, it is noteworthy that the payload threshold values of the 7.8 mm robot from Figs. 6 and 7 are both around 3 g, i.e., when Δz change from positive to negative.

Results for Robot Dynamics: Table III-C summarises the identified dynamic parameters of the second- or third-order systems for the two robots. Fig. 8 (a) illustrates the step response of the applied pressure. The dynamics of the real pressure behave in a first-order system manner, with an identified time constant τ of 0.085 s. Fig. 8 (b) suggests that the soft robot exhibits different dynamic behaviour when different robotic segments are actuated. For instance, the robot is over-damped when only the second segment is actuated.

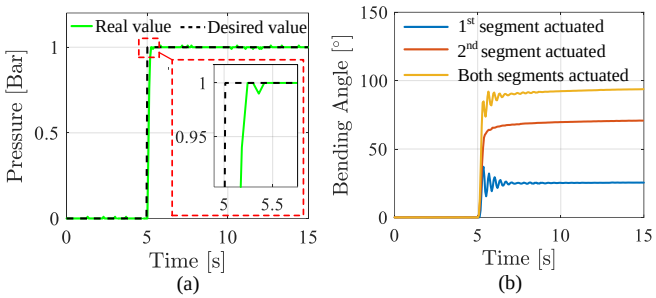

Fig. 8. Results for Experiment 3: Illustration of (a) the applied step pressure and (b) different dynamic bending behaviours of the 7.8 mm robot when the first, second, and both segments are actuated.

Conversely, the robot is under-damped when the first segment or when both segments are actuated. Therefore, the second-order and third-order systems are used to describe the under-damped and over-damped dynamic behaviour, respectively. Moreover, the robot dynamics are also dependent on the numbers of the actuated chambers, as demonstrated in Fig.9 and Table III-C.

Fig. 9 details the step response of the identified dynamic systems. It is observed that the two robots show similar dynamic bending behaviour, but the 9.5 mm robot has a larger gain factor k than that of the 7.8 mm robot. Fig. 9(a) shows that robots have the greatest settling time of 2.0 s $\sim$ 3.0 s when only the first segment is actuated. In contrast, the settling time from Fig. 9(a) is about 1.0 s. In addition, the results show that the number of the actuated chambers primarily influence the gain factor k. For example, the natural frequencies of the second segment of the 9.5 mm robot are 8.7 Hz and 7.9 Hz, subject to one chamber and two chambers actuation. Similarly, these two frequencies of the 7.8 mm robot are 8.1 Hz and 7.9 Hz. In addition, when the second segment is actuated, the damping factor is between 1.0 and 1.2 when two robots bend. Meanwhile, the damping factor for the elongation motion is 1.2$\sim$1.3. Comparing Fig. 9(a) to Fig. 9(b), the overshot is not observed when both segments are actuated. In all bending and elongation tests, the gain factor k of the 9.5 mm robot is larger than that of the 7.8 mm robot, as evidenced by the parameters from Table III-C.

Results for Burst Pressure Evaluation: Fig. 10 reports the results of the burst pressure evaluation as tested on the smaller 7.8 mm robot. The robot doesn't experience explosion or pressure leakage under extreme conditions, as the real pressure follows desired pressure and reaches 2.95 bar. It is noteworthy that the actuated chamber starts to wrinkle when the pressure exceeds 2.5 bar.

IV. DISCUSSIONS

The fabrication process outlined in this work is essential for creating these miniaturised soft robots. Comparing it to the fabrication approach introduced in [15], [24], we

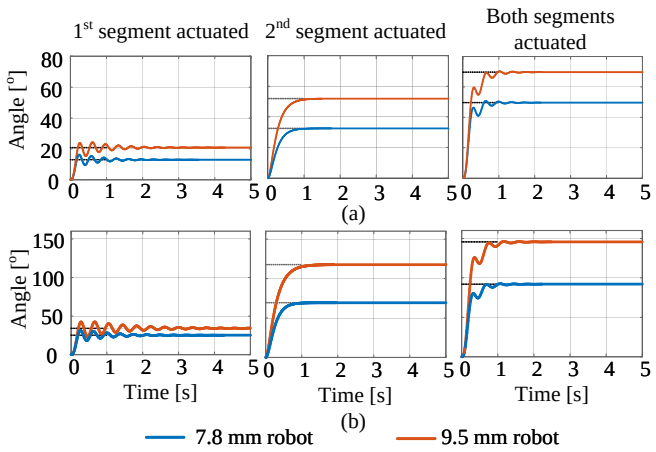

Fig. 9. Results for Experiment 3: Step response of identified transfer functions (see Table III-C) for two robots under (a) one chamber and (b) two chambers actuation. In the illustration of the step response, the input is a step pressure of 1.0 bar and the output is the resulting bending angle.

see that the inner chamber moulds in this work are one-piece rods (see Fig. 3(a)) rather than assembled moulds. Indeed only eight printed mould parts are required in this work, reducing the number of mould parts, thereby avoiding unexpected deformation resulting from post-curing of printed parts. The smallest rod, used in the fabrication of our 7.8 mm robot, has a diameter of 1.0 mm. Another potential inner chamber mould could take advantage of carbon-fibre rods [35] whose diameter can be as small as 0.5 mm, potentially leading to further miniaturisation of these soft robots. As presented in Section II-A, the selection of the outermost diameters for robots relies on the trocar ports. Additionally, the design of chamber diameters must account for the dimensions of available metal rods. It is noteworthy that when the wall thickness δ_c is below 0.4 mm, there is an increased susceptibility to failure in the fabrication of the inner chamber layer (refer to Fig. 3). To ensure a consistent and reliable mould positioning during assembly, alignment slots have been incorporated into our moulds. It is worth mentioning that fabrication inconsistency might exist, e.g., arising from the manually-woven reinforcement layer.

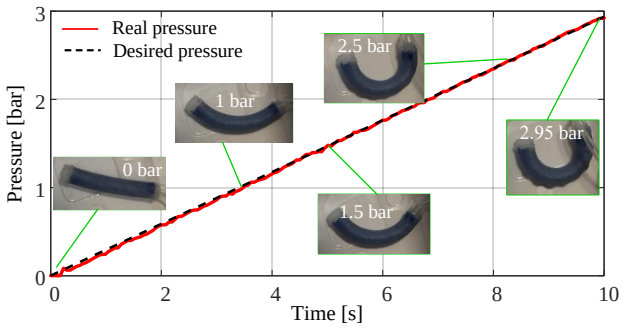

Fig. 10. Results for Experiment 4: Burst pressure evaluation. The 7.8 mm robot doesn't exhibit burst, and the real chamber pressure follows the desired pressure from 0 bar to 2.95 bar.

Experiment 1 demonstrates that the 9.5 mm robot can achieve similar bending angles or elongation distances to the 7.8 mm robot, but at lower pressure. This is due to the fact that the cross-sectional area of the actuation chamber of the 9.5 mm robot is 2.25 times larger than the area of the 7.8 mm robot. Similar to other large-scale soft robots [26], Fig. 4 shows that these miniaturised soft robots also exhibit non-negligible hysteresis when they bend or elongate under various pressures. This inherent hysteresis might result from a combination of the viscoelasticity of the silicone material, the friction between reinforcement cords and the silicone matrix, and the friction between reinforcement cords themselves [36]. In addition, the bending angles resulting from three chamber actuation are smaller than the angles produced from two chamber actuation. This is explained by the fact that two of the three actuated chambers generate elongation, and the rest of the actuated chamber generates bending moments.

Experiment 2 illustrates that the two robots have different payload capabilities, which itself is dependent on the numbers of actuated chambers and segments. Compared to the 7.8 mm robot, the 9.5 mm robot has better force capabilities. The difference stems from the fact that the 9.5 mm robot has greater flexural strength resulting from a larger second moment of area. Figs. 6 and 7 highlight that the lifting height Δz could be less than zero, especially in the case that three chambers are actuated. This can be explained by the fact that the overall stiffness of soft robots decreases as their elongation ratio increases [34]. As such, it would be advisable to consider the number of actuated chambers when dealing with payloads, i.e, actuating just two chambers to generate better payload capability.

Experiment 3 reveals that the identification of dynamics of soft robots should also consider the dynamic behaviours of the actuation pressure properly (see Fig. 8). The dynamics of pressure usually depends on the controller and the pipe length. In our case, the identified time constant τ is 0.085 s, using Camozzi pressure regulators and setting lengths of 4 mm diameter pipe as 1 m. In addition, the dynamics of soft robots is also impacted by the actuated segments and robot dimensions [37], as reported in Fig. 9. For example, when only the second segment is actuated, the system dynamics exhibit under-damped behaviour, whereas oscillations are evident if only the first segment is activated. This can be explained by the fact that the inertia of the second segment will increase the overall inertia of the first segment when it is actuated. Conversely, the first segment exerts no impact on the inertia of the actuated second segment.

Experiment 4 shows that the fabricated soft robot is robust to extreme pressure. Specifically, the smaller soft robot can endure a pressure of 2.95 bar without explosion or leakage (see Fig. 10). Please note that 3.0 bar is the nominal controllable pressure from the manufacturer. We found that 2.95 bar was the maximum achievable pressure in our experimental setup. This difference of 0.05 bar might result from, extraneous factors such as resistor tolerances from the amplification circuits.

V. Conclusions

This paper presents miniaturised soft manipulators on the sub-centimetre scale, with fully reinforced actuation chambers and a free central lumen. Specifically, two robots with diameters of 9.5 mm and 7.8 mm are discussed, from robot fabrication to robot characterisation. Each has two segments and eight actuation chambers in total. The experimental characterisation clearly reveals the properties of these robots in terms of bending and elongation, force capability, dynamics and robustness to extreme pressure.

Progress in the miniaturisation of soft manipulators with reinforced chambers and a free lumen is propelled by the achievements reported in this study. Successful miniaturisation provides new insights in relation to the use of these soft robots in a wide range of medical applications, e.g., endoscopic intervention. In the future, we will look into the creation and control of miniaturised soft medical instruments with other integrated components, e.g., cameras, laser fibres or proprioceptive sensing devices.

References

[1] A. D. Marchese, R. K. Katzschmann, and D. Rus, "A recipe for soft fluidic elastomer robots," *Soft Robotics*, vol. 2, no. 1, pp. 7–25, 2015.

[2] J. Peters *et al.*, "Hybrid fluidic actuation for a foam-based soft actuator," in *IEEE/RSJ International Conference on Intelligent Robots and Systems (IROS)*, 2020, pp. 8701–8708.

[3] J. Peters, E. Nolan *et al.*, "Actuation and stiffening in fluid-driven soft robots using low-melting-point material," in *IEEE/RSJ International Conference on Intelligent Robots and Systems (IROS)*, 2019, pp. 4692–4698.

[4] Y. Sun *et al.*, "Stiffness customization and patterning for property modulation of silicone-based soft pneumatic actuators," *Soft Robotics*, vol. 4, no. 3, pp. 251–260, 2017.

[5] F. Connolly, P. Polygerinos, C. J. Walsh, and K. Bertoldi, "Mechanical programming of soft actuators by varying fiber angle," *Soft Robotics*, vol. 2, no. 1, pp. 26–32, 2015.

[6] R. H. Gaylord, "Fluid actuated motor system and stroking device," 1958, US Patent 2,844,126.

[7] B. Tondu, "Modelling of the mckibben artificial muscle: A review," *Journal of Intelligent Material Systems and Structures*, vol. 23, no. 3, pp. 225–253, 2012.

[8] K. Suzumori, S. Iikura, and H. Tanaka, "Applying a flexible microactuator to robotic mechanisms," *IEEE Control Systems Magazine*, vol. 12, no. 1, pp. 21–27, 1992.

[9] K. Suzumori *et al.*, "Development of flexible microactuator and its applications to robotic mechanisms," in *IEEE International Conference on Robotics and Automation (ICRA)*, 1991, pp. 1622–1623.

[10] K. Suzumori, S. Endo, T. Kanda, N. Kato, and H. Suzuki, "A bending pneumatic rubber actuator realizing soft-bodied manta swimming robot," in *IEEE International Conference on Robotics and Automation (ICRA)*, 2007, pp. 4975–4980.

[11] Z. Gong *et al.*, "A soft manipulator for efficient delicate grasping in shallow water: Modeling, control, and real-world experiments," *The International Journal of Robotics Research*, vol. 40, no. 1, pp. 449–469, 2021.

[12] J. Fras, Y. Noh, H. Wurdemann, and K. Althoefer, "Soft fluidic rotary actuator with improved actuation properties," in *IEEE/RSJ International Conference on Intelligent Robots and Systems (IROS)*, 2017, pp. 5610–5615.

[13] J. Zhang *et al.*, "Fiber-reinforced soft polymeric manipulator with smart motion scaling and stiffness tunability," *Cell Reports Physical Science*, vol. 2, no. 10, 2021.

[14] P. Polygerinos *et al.*, "Modeling of soft fiber-reinforced bending actuators," *IEEE Transactions on Robotics*, vol. 31, no. 3, pp. 778–789, 2015.

[15] J. Fraś *et al.*, "New STIFF-FLOP module construction idea for improved actuation and sensing," in *IEEE International Conference on Robotics and Automation (ICRA)*, 2015, pp. 2901–2906.

[16] F. Lamping, D. Müller, and K. M. de Payrebrune, "A systematically derived design for a modular pneumatic soft bending actuator," in *IEEE International Conference on Soft Robotics (RoboSoft)*, 2022, pp. 41–47.

[17] D. Trivedi, A. Lotfi, and C. D. Rahn, "Geometrically exact dynamic models for soft robotic manipulators," in *IEEE/RSJ International Conference on Intelligent Robots and Systems (IROS)*, 2007, pp. 1497–1502.

[18] Y. Zhang, T. Wang, W. He, and S. Zhu, "Human-powered master controllers for reconfigurable fluidic soft robots," *Soft Robotics*, vol. 10, no. 6, pp. 1126–1136, 2023.

[19] K.-W. Kwok *et al.*, "Soft robot-assisted minimally invasive surgery and interventions: Advances and outlook," *Proceedings of the IEEE*, vol. 110, no. 7, pp. 871–892, 2022.

[20] A. Arezzo *et al.*, "Total mesorectal excision using a soft and flexible robotic arm: a feasibility study in cadaver models," *Surgical Endoscopy*, vol. 31, pp. 264–273, 2017.

[21] M. Cianchetti *et al.*, "Soft robotics technologies to address shortcomings in today's minimally invasive surgery: the STIFF-FLOP approach," *Soft Robotics*, vol. 1, no. 2, pp. 122–131, 2014.

[22] J. Shi *et al.*, "Screw theory-based stiffness analysis for a fluidic-driven soft robotic manipulator," in *IEEE International Conference on Robotics and Automation (ICRA)*, 2021, pp. 11 938–11 944.

[23] A. Shiva *et al.*, "Tendon-based stiffening for a pneumatically actuated soft manipulator," *IEEE Robotics and Automation Letters*, vol. 1, no. 2, pp. 632–637, 2016.

[24] H. Abidi *et al.*, "Highly dexterous 2-module soft robot for intra-organ navigation in minimally invasive surgery," *The International Journal of Medical Robotics and Computer Assisted Surgery*, vol. 14, no. 1, p. e1875, 2018.

[25] J. Shi, S. Abad Guaman, J. Dai, and H. Wurdemann, "Position and orientation control for hyperelastic multisegment continuum robots," *IEEE/ASME Transactions on Mechatronics*, pp. 1–12, 2024.

[26] J. Shi, W. Gaozhang, and H. A. Wurdemann, "Design and characterisation of cross-sectional geometries for soft robotic manipulators with fibre-reinforced chambers," in *IEEE International Conference on Soft Robotics (RoboSoft)*, 2022, pp. 125–131.

[27] P. Chaillou *et al.*, "Reduced finite element modelling and closed-loop control of pneumatic-driven soft continuum robots," in *IEEE International Conference on Soft Robotics (RoboSoft)*, 2023, pp. 1–8.

[28] E. Almanzor *et al.*, "Static shape control of soft continuum robots using deep visual inverse kinematic models," *IEEE Transactions on Robotics*, vol. 39, no. 4, pp. 2973–2988, 2023.

[29] S.-A. Abad, A. Arezzo, S. Homer-Vanniasinkam, and H. A. Wurdemann, "Soft robotic systems for endoscopic interventions," in *Endorobotics*. Elsevier, 2022, pp. 61–93.

[30] G. Fang *et al.*, "Soft robotic manipulator for intraoperative MRI-guided transoral laser microsurgery," *Science Robotics*, vol. 6, no. 57, p. eabg5575, 2021.

[31] A. B. Dawood *et al.*, "Fusing dexterity and perception for soft robot-assisted minimally invasive surgery: What we learnt from STIFF-FLOP," *Applied Sciences*, vol. 11, no. 14, p. 6586, 2021.

[32] I. Alkatout *et al.*, "Abdominal anatomy in the context of port placement and trocars," *Journal of the Turkish German Gynecological Association*, vol. 16, no. 4, p. 241, 2015.

[33] J. Shi, W. Gaozhang, H. Jin, G. Shi, and H. A. Wurdemann, "Characterisation and control platform for pneumatically driven soft robots: Design and applications," in *IEEE International Conference on Soft Robotics (RoboSoft)*, 2023, pp. 1–8.

[34] J. Shi *et al.*, "Stiffness modelling and analysis of soft fluidic-driven robots using Lie theory," *The International Journal of Robotics Research*, vol. 43, no. 3, pp. 354–384, 2024.

[35] Y. Sun, S. Song, X. Liang, and H. Ren, "A miniature soft robotic manipulator based on novel fabrication methods," *IEEE Robotics and Automation Letters*, vol. 1, no. 2, pp. 617–623, 2016.

[36] T. Vo-Minh, T. Tjahjowidodo, H. Ramon, and H. Van Brussel, "A new approach to modeling hysteresis in a pneumatic artificial muscle using the maxwell-slip model," *IEEE/ASME Transactions on Mechatronics*, vol. 16, no. 1, pp. 177–186, 2011.

[37] A. Shariati, J. Shi, S. Spurgeon, and H. A. Wurdemann, "Dynamic modelling and visco-elastic parameter identification of a fibre-reinforced soft fluidic elastomer manipulator," in *IEEE/RSJ International Conference on Intelligent Robots and Systems (IROS)*, 2021, pp. 661–667.